Thermal diffusivity determination using heterodyne phase insensitive transient grating spectroscopy

Citation: Dennett, Cody A., and Michael P. Short. "Thermal Diffusivity Determination Using Heterodyne Phase Insensitive Transient Grating Spectroscopy." Journal of Applied Physics 123, no. 21 (June 7, 2018): 215109.

As Published: http://dx.doi.org/10.1063/1.5026429

Persistent URL: http://hdl.handle.net/1721.1/118413

Version: Author's final manuscript: final author's manuscript post peer review, without publisher's formatting or copy editing

This manuscript was accepted by J. Appl. Phys. Click here to see the version of record.

Thermal diffusivity determination using heterodyne phase insensitive transient grating spectroscopy

Cody A. Dennett* and Michael P. Short
Department of Nuclear Science and Engineering,
Massachusetts Institute of Technology, Cambridge, MA 02139, USA
(Dated: May 3, 2018)

The elastic and thermal transport properties of opaque materials may be measured using transient grating spectroscopy (TGS) by inducing and monitoring periodic excitations in both reflectivity and surface displacement. The 'phase grating' response encodes both properties of interest, but complicates quantitative analysis by convolving temperature dynamics with surface displacement dynamics. Thus, thermal transport characteristics are typically determined using the 'amplitude grating' response to isolate the surface temperature dynamics. However, this signal character requires absolute heterodyne phase calibration and contains no elastic property information. Here, a method is developed by which phase grating TGS measurements may be consistently analyzed to determine thermal diffusivity with no prior knowledge of the expected properties. To demonstrate this ability, the wavelength-dependent 1D effective thermal diffusivity of pure germanium is measured using this type of response and found to be consistent with theoretical predictions made by solving the Boltzmann transport equation. This ability to determine elastic and acoustic properties from a single set of TGS measurements will be particularly advantageous for new *in situ* implementations of the technique being used to study dynamic materials systems.

I. INTRODUCTION

Optically heterodyne amplified transient grating spectroscopy (TGS) measurements are a powerful tool used in the study of surface thermal transport [1], elastic mechanical performance [2], film properties [3–6], and a variety of other dynamic processes [7–9]. TGS has proven a particularly useful tool for studying the properties of heterostructures [10] as well as short-wavelength, non-ballistic heat transport in semiconductors [11]. Recently, TGS has become of particular interest in the study of the effects of ion irradiation on material properties, as the micron-scale excitations imposed can be tuned to match the length scale of imposed damage profiles [12–15]. Advances in time-resolved implementations of this and similar methods have drawn attention as potential *in situ* measurement tools given their ability to recover elastic and thermal properties using a non-contact and non-destructive methodology [16,17].

In common implementations, TGS uses two pulsed lasers crossed at the surface of a sample under interrogation to generate a pulsed, spatially periodic intensity pattern on this surface. Laser heating in this periodic pattern induces a periodic material excitation in both temperature and surface displacement, $u(t)$, due to thermal expansion. In most materials, the complex reflectivity, $r^*(t) = r_0[1 + r'(t) + ir''(t)]$, is temperature-dependent, indicating that periodic 'gratings' in both reflectivity and surface displacement will be present following excitation. The dynamics of these gratings are monitored by recording the intensity of the first order diffraction of a quasi-continuous wave probing laser from the surface gratings.

In the 'boxcar' geometry used for TGS measurements made here [18], the diffracted signal is spatially overlapped with a reference oscillator to heterodyne amplify the recorded signal. Johnson, et al. showed that the total optical intensity of heterodyne response for TGS measurement made in the 'reflection geometry', i.e. for opaque materials, is given by

$$I(t,\phi) = t_r I_{0p} R_0 [r'(t)\cos\phi - (r''(t) - 2k_p u(t)\cos\beta_p)\sin\phi], \quad (1)$$

where I_{0p} is the initial intensity of both the reference oscillator and probing beams, t_r is the attenuation factor of the neutral density filter normally placed in the reference oscillator path, $R_0 = |r_0|^2$ is the reflectivity of the sample, k_p is the optical wave vector, β_p is the angle of incidence of the probe beams onto the sample surface (as shown in Fig. 1), and ϕ is the heterodyne phase difference between the reference and probe beams [1].

Eq. (1) holds only in the regime where the reference oscillator intensity is much greater than the diffracted signal intensity, which is true in TGS experiments. This form indicates that by setting the heterodyne phase in experiment to $\phi = 0$ or $\phi = \pi$, the real component of the reflectivity change, $r'(t)$, may be isolated. This selection of phase is referred to as the 'amplitude grating.' If the phase is chosen to be $\phi = \pm\pi/2$, the 'phase grating' may be selected, which is comprised of a combination of the imaginary part of the reflectivity, $r''(t)$, and the surface displacement, $u(t)$. Both the gratings in reflectivity and displacement will thermally equilibrate following excitation, with decay rates determined by the thermal diffusivity of the material in question and the wavelength of the imposed excitation, Λ. The surface displacement component may contain one or more surface acoustic oscillations depending on the surface structure and composition of the material in question. It is these acoustic modes which may be analyzed to deter-

* cdennett@mit.edu

mine information like elastic properties and surface layering structure [3,19].

Given the ability to isolate the reflectivity dynamics in the amplitude grating response, most authors choose this signal character when measuring thermal performance using TGS [1,11]. However, amplitude grating measurements require absolute heterodyne phase calibration and only contain information regarding thermal transport characteristics. The phase grating response, in contrast, allows for simultaneous determination of both thermal and acoustic properties. This is a distinct advantage for time-resolved, *in situ* TGS implementations seeking to retain as much information about sample performance as possible in a single set of measurements. Measurements made in this manner also have the advantage of being insensitive to deviations in the heterodyne phase at which data is collected, rendering experimental measurement of thermal transport easier to implement in practice. In this work, a method is constructed by which a determination of thermal performance may be made using phase grating measurements. The method proposed here is benchmarked by measuring the grating-wavelength-dependent thermal diffusivity of pure Ge from $\Lambda = 3.6$ to 9.8 µm. Measured values of thermal diffusivity are compared to the expected thermal diffusivity at these wavelengths as computed using a variational solution to the Boltzmann transport equation and found in good agreement. Using this analysis, best practices are recommended for phase grating thermal transport determination in future studies.

II. METHODS

To investigate the thermal performance characterization using phase grating TGS, a series of measurements are carried out on pure, un-doped, germanium single crystals purchased from the MTI corporation. Three single crystals with surface orientations {001}, {011}, and {111}, each polished to a surface roughness of <8 Å are used. TGS measurements are carried out along primary surface directions $\langle 100\rangle\{001\}$, $\langle 11\bar{1}\rangle\{011\}$, and $\langle 11\bar{2}\rangle\{111\}$ by fixing the rotation of the sample with respect to the optical arrangement. These directions are indicated by the manufacturer and confirmed by comparing the measured surface acoustic wave velocity to values computed for these surface directions using elastic theory [20,21]. In materials with phonon-dominated thermal transport, several authors have shown that thermal diffusivities measured using short-wavelength excitations, like those used in TGS, will be smaller than bulk diffusivities [4,11]. In brief, this reduction occurs due to the exclusion of long-wavelength ballistic phonons from the heat transport process. For SiGe alloys, Huberman et al. have implemented a variational approach to solving the Boltzmann transport equation (BTE) for short-wavelength, 1D periodic excitations [11]. That method allows for the calculation of the expected value of the effective thermal diffusivity in pure Ge comfortably including the normal operating range of TGS test wavelengths of $\Lambda = 1-10$ µm. Using these calculated values as a benchmark, phase grating thermal transport measurements may be quantified by collecting data at a variety of TGS wavelengths on only a small number of samples.

Experimental TGS measurements are made using a dual heterodyne phase collection (DH-TGS) optical geometry [17]. A schematic diagram of the optical arrangement used for these experiments is shown in Fig. 1. Excitations are generated using a passively Q-switched, 532 nm, solid state laser with a pulse length of 300 ps, and a repetition rate of 1 kHz as a pump laser (TEEM Photonics STG-03E-120). At the sample surface, the laser spot size is 140 µm. The probing laser source is a 785 nm, CW diode laser (Thorlabs LD785-SEV300 with controller LTC100-B) modulated to a repetition rate of 1 kHz with a 25% duty cycle using an optical chopper wheel and a spot size at the sample surface of 105 µm. The probe laser is RF modulated in this way to reduce sample heating while matching the repetition rate of the pump laser. Silicon avalanche photodiodes (Hamamatsu C5658) with a 50 kHz–1 GHz bandwidth are used to detect the heterodyne-amplified probe signal. Their outputs are concurrently recorded on a dual-band 5 GHz digital oscilloscope. Each measurement is taken as the average of 10000 laser shots to reduce noise. All measurements are made in rough vacuum (< 15 mTorr) to remove the possibility of exiting acoustic oscillations in air near the sample surface.

A variety of TGS test wavelengths may be chosen in experiment using a custom volumetric diffraction optic with many etched patterns. Each pattern, in conjunction with the optical geometry, fixes the nominal wavelength, Λ_0, at which the periodic excitation is projected [18]. However, as minor misalignments may affect this projected grating spacing, the actual projected grating is calibrated before experiments at each wavelength using a tungsten reference sample with a known surface acoustic wave speed. Here, six grating spacings are used ranging from 3.6 to 9.8 µm and the maximum deviation of any of the calibrated grating spacings from the nominal grating spacings is measured at 0.28%. Measurements will be referred to in the text by their nominal grating spacings, though for each fit the calibrated spacing is used as a fixed parameter. At 3.6, 4.8, and 6.4 µm, 10 measurements are made on each of the three single crystal orientations for a total of 30 points per grating spacing. Each measurement point is mechanically translated across the sample surface to provide a spatial average. Analysis of these measurements shows no statistical difference between values of thermal diffusivity measured on each sample. Therefore, the remaining measurements at 5.5, 8.5, and 9.8 µm were carried out solely on the {001} Ge crystal, using 30 spatially separated spots each.

Effective thermal diffusivities are extracted from TGS measurements using non-linear least squares curve fitting. All fitting and analysis is conduced here using

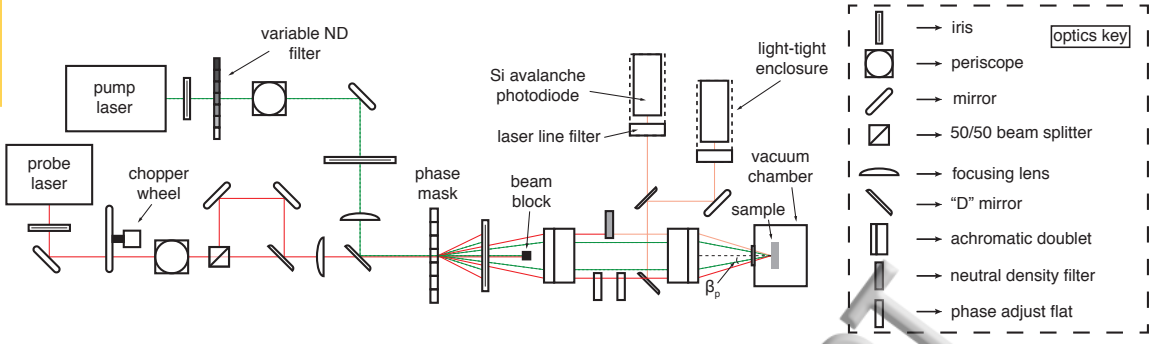

FIG. 1. Top-view schematic diagram of DH-TGS arrangement used in this work. Following the beam splitter in the probe path, the two vertically separated probe beams are not rendered. The angle of incidence of the probe beams, β_p, onto the sample surface is indicated. More details on the optical arrangement can be found in [17].

the MATLAB platform (version R2016b, Mathworks Inc.) using the ability to fit to arbitrary, user-defined functional forms. All fits are un-weighted and computed using the Levenberg-Marquardt algorithm [22]. Best-practices described herein are referred to using non-platform-specific terms and may be implemented using any scientific data analysis tool. All original data files, scripts used to process them, and resultant measurements can be found in the permanent GitHub repository for this manuscript [23].

III. GRATING THERMAL TRANSPORT

In order to extract thermal property information from TGS measurements, the temperature and displacement dynamics resulting from an infinite 1D periodic excitation have been analytically investigated. Kading, et al. showed that in the limit of surface energy absorption and isotropic thermal diffusivity the surface temperature dynamics, and therefore the reflectivity dynamics, of a grating excited by a delta function laser impulse should follow

$$\{r'(t), r''(t)\} \propto \frac{1}{\sqrt{t}} \exp\left(-q^2 \alpha t\right), \tag{2}$$

where α is the isotropic thermal diffusivity and $q = 2\pi/\Lambda$ is the imposed grating wave vector [24]. In the same limits, the surface displacement takes a profile of the form

$$u(t) \propto \operatorname{erfc}\left(q\sqrt{\alpha t}\right), \tag{3}$$

where $\operatorname{erfc}(\cdot)$ is the complimentary error function. As the penetration depth of the 532 nm laser excitation is about 9 nm in Ge, this surface excitation approximation is good for the material system considered here [25]. Similarly, the isotropic diffusivity approximation is appropriate for bulk materials with cubic symmetry, but may fail for systems with hexagonal symmetry or heterostructures. These forms have both been used with success to determine thermal diffusivities from TGS experiments [1,4,13]. In practice, TGS measurements often make use of the heterodyne phase dependence in Eq. (1) to construct a composite trace which is the difference of two measurements made at complimentary heterodyne phases such that

$$\begin{aligned} I^{\text{tot}}(t) &= I(t,\phi_1) - I(t,\phi_2) \\ &\propto [r'(t)\,(\cos\phi_1 - \cos\phi_2) \\ &\quad - (r''(t) - 2k_p u(t)\cos\beta_p)\,(\sin\phi_1 - \sin\phi_2)]\,. \end{aligned} \tag{4}$$

In this manner, systematic background noise may be removed from the composite measurement without changing the dynamics of the response.

A. The amplitude grating

Using the construction of Eq. (4), complete amplitude grating measurements may therefore be collected by making two measurements at $\phi_1 = 0$ and $\phi_2 = \pi$ either sequentially or concurrently using the dual heterodyne phase collection geometry [17]. Since the grating wave vector, q, is fixed by the experiment, this composite trace may be fit using non-linear least squares optimization to the form

$$I_A(t) = \frac{A}{\sqrt{t}} \exp(-q^2\alpha t) + B, \tag{5}$$

where A and B are constants, to uniquely determine the thermal diffusivity of the sample in question. This method has been used to study thermal transport in a variety of systems including thick PbTe films [1], bulk SiGe alloys [11], and bulk GaAs [26]. However, as mentioned above, measurements of this type do not retain any information related to acoustic properties as those properties are uniquely contained in $u(t)$. In addition, measurements made in this manner rely on an absolute calibration of the heterodyne phase used in experiment, which is practice is quite difficult. If measurements are collected at heterodyne phases off from 0 or π, some contribution to the signal intensity will be made by the displacement response and fitting to Eq. (5) will not return the correct

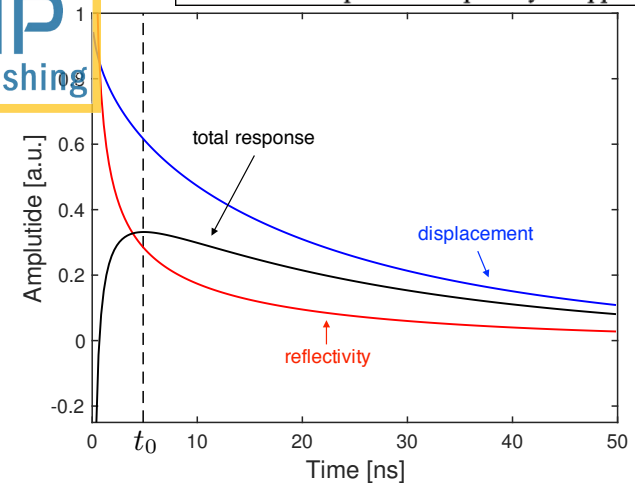

FIG. 2. Components of the phase grating thermal transport model calculated using Eq. (6). Parameters are extracted from one measurement point on a {111} Ge sample as $\Lambda = 6.39$ µm, $\alpha = 0.267$ cm^2/s, and $\beta = 2.25 \times 10^{-5}$ s$^{1/2}$.

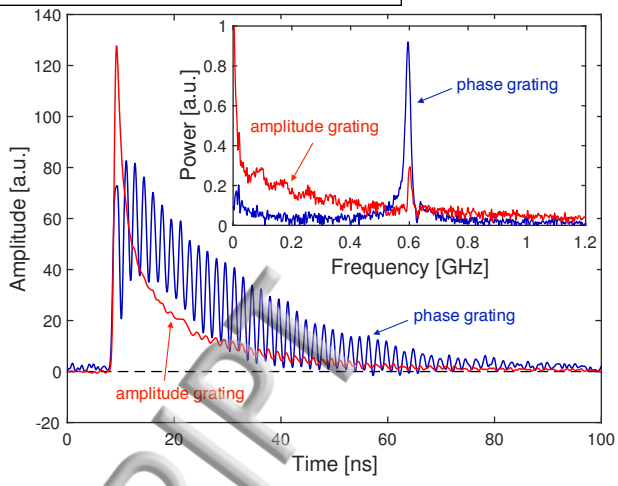

FIG. 3. Experimental amplitude and phase grating data for $\Lambda_0 = 4.8$ µm on a {011} Ge crystal. The inset shows the filtered Fourier transform of both amplitude and phase grating responses. The retention of a small peak in the Fourier transform of the amplitude grating data indicates either a slight offset in the heterodyne phase or a small pump/probe spatial mismatch.

value for thermal diffusivity. Johnson, et al. note this strict phase requirement and recommend the use of a reference sample for phase calibration [1]. Absolute optical measurements of heterodyne phase without the use of a reference sample are possible, but implementing these methods may not be practical for all applications [27].

B. The phase grating

In comparison, making a complete phase grating measurement requires taking the difference of two measurements made at $\phi_1 = \pi/2$ and $\phi_2 = -\pi/2$. Excluding the contribution of $u(t)$ due to acoustic oscillation, the complete phase grating signal is given by

$$I_P(t) = A\left[\mathrm{erfc}\left(q\sqrt{\alpha t}\right) - \frac{\beta}{\sqrt{t}}\exp\left(-q^2\alpha t\right)\right] + B, \quad (6)$$

where β is a constant describing the ratio of displacement and reflectivity contributions and A and B are again amplitude constants. Fig. 2 shows the displacement, reflectivity, and complete phase grating response calculated based on Eq. (6) for best-fit parameters from a measurement at 6.39 µm on Ge, and Fig. 3 shows measured amplitude and phase grating data for an excitation wavelength of 4.8 µm.

Unlike amplitude grating measurements, Eq. (6) is robust against small changes in heterodyne phase. A phase grating measurement made at $\phi_1 = \pi/2 + \delta_1$ and $\phi_2 = -\pi/2 + \delta_2$ for $\delta_i \ll \pi/2$ will, by Taylor expansion, follow

$$\begin{aligned} I^{\mathrm{tot}} &= A\left[u(t) + cr'(t)(\delta_1 + \delta_2) - dr''(t)\right] + B \\ &= A\left[\mathrm{erfc}\left(q\sqrt{\alpha t}\right) + \frac{c\,(\delta_1+\delta_2) - d}{\sqrt{t}}\exp\left(-q^2\alpha t\right)\right] + B \\ &= A\left[\mathrm{erfc}\left(q\sqrt{\alpha t}\right) - \frac{\beta}{\sqrt{t}}\exp\left(-q^2\alpha t\right)\right] + B \end{aligned} \quad (7)$$

where c and d above are constants which may be combined with the phase offsets δ_i to give the fitting constant β. This expression is, of course, the same form as Eq. (6). Therefore, in practice, phase grating measurements need be made only by roughly optimizing the heterodyne phase to the correct value and thermal parameters may still be extracted.

This approximate optimization may be conducted by making use of the acoustic component of $u(t)$. These oscillations are evident in Fig. 3, and the inset shows the Fourier transform of the response, by which the dominant frequencies may be easily identified. By adjusting ϕ to $\pm\pi/2$, the amplitude of these acoustic oscillations will be maximized. By using the real-time Fourier transform capability of any modern digital oscilloscope, ϕ may be set and manually optimized to very close to this value by maximizing the intensity of the peak due to acoustic oscillations. Phase grating responses optimized in this manner do not require absolute phase calibration, and thermal diffusivities fit to such profiles are insensitive to small deviations in heterodyne phase. All phase grating measurements carried out here use this method of optimization.

This manuscript was accepted by J. Appl. Phys. Click here to see the version of record.

C. Parameter estimation

Two major difficulties arise in naïvely using a standard non-linear least squares optimization algorithm with Eq. (6) to extract thermal diffusivity values from TGS measurements. The presence of the imposed acoustic oscillation from $u(t)$ is not taken into account in Eq. (6) and complicates finding robust optimal values for α. This detail is discussed at length in Section IV. Additionally, for some values of α and β a naïve fit will tend to ignore the maximum in the thermal response profile seen at t_0 in Fig. 2. In these cases, the value of β is underestimated; the fit parameters represent a local minimum and will not return an accurate value for α. This tendency can be overcome by providing a good initial guess for both α and β, which is often possible when measuring materials with known or expected properties.

However, for materials with unknown properties, providing these initial estimations may be problematic. In these cases, it is possible to pre-compute initial guesses for α and β. For profiles with a maximum present, the location of t_0 can be found analytically by solving

$$\left.\frac{\partial I_P(t)}{\partial t}\right|_{t_0} = 0, \tag{8}$$

which yields the following expression for t_0:

$$t_0 = \frac{\beta}{2}\left[\frac{q\sqrt{\alpha}}{\sqrt{\pi}} - \beta q^2\alpha\right]^{-1}. \tag{9}$$

By noting that this expression is only physically meaningful if $t_0 > 0$, the maximum value of β possible for this feature to appear is

$$\beta_{\max} = \frac{1}{q\sqrt{\pi\alpha}}, \tag{10}$$

for a measurement conducted with a given value of q on a material with a thermal diffusivity α. This expression becomes of use when noting that simple maxima may be easily identified using standard data processing tools. Therefore, when attempting to extract values for thermal diffusivity from TGS measurements with no prior knowledge of the expected value (like the phase grating measurement in Fig. 3), we may pre-compute guesses for α and β using a simple algorithm and by noting that Eq. (9) may be inverted to read

$$\beta = \frac{q\sqrt{\alpha}}{\sqrt{\pi}}\left[q^2\alpha + \frac{1}{2t_0}\right]^{-1}. \tag{11}$$

The pre-computation algorithm then proceeds by the following steps:

1. Find t_0 from the measured response by taking the location of the absolute maximum of the profile.
2. Perform an initial fit to the measured data using solely an erfc$(\cdot)$ to describe the thermal decay. This provides a initial estimation for α.
3. Calculate an initial estimate of β using Eq. (11), t_0, and the initial estimate of α.
4. Re-fit the measured response to the form of Eq. (6) by fixing β to the calculated value and varying only α.
5. From the new value of α, re-compute β using Eq. (11) and t_0.
6. Iterate steps 4 and 5 until the values of α and β converge.

For an idealized thermal decay which includes no acoustic oscillation, this procedure should converge to the true value of α and β. However, the acoustic oscillation normally included in $u(t)$ most often causes a value of t_0 to be found which is close to, but not the true value of t_0 as determined by Eq. (9). However, these values may be taken as initial guesses in a full fit of Eq. (6), allowing all four parameters (A, B, α, and β) to vary. It is the output of this final fit which is indicative of the true value of thermal diffusivity for a given TGS measurement. All analysis carried out here uses this pre-computation method with a fixed number of iterations (10, in this case) to supply starting points for the optimization of α for each profile.

D. Acoustic oscillations

Previously, Hofmann et al. have used phase grating TGS measurements to determine changes in the thermal performance of ion irradiated tungsten [13]. In their case, phase grating measurements were necessary due to the lack of a discernible amplitude grating response. Physically, this indicates that there is very little change in the reflectivity of tungsten as a function of temperature. This allowed them to fit phase grating measurements to a form of Eq. (3) only, without needing to include the second term present in Eq. (6). They noted that the best fit value of α from their procedure seemed to depend on the starting point at which the profile was fit with respect to the observed acoustic oscillation. However, by fitting their data to Eq. (3) with the addition of a decaying sinusoidal oscillation, the variation in the best-fit value of α at different fit start times was reduced.

This variation in best-fit value with fit starting time is also observed in the data collected here, which includes a non-negligible contribution in reflectivity change in the phase grating response. Therefore, like Hofmann et al., data here are also fit with the addition of a decaying sinusoidal contribution to account for acoustic oscillations. Following parameter pre-computation, the final fit to experimental data is of the form

$$\begin{aligned} I_P(t) = A\left[\mathrm{erfc}\left(q\sqrt{\alpha t}\right) - \frac{\beta}{\sqrt{t}}\exp\left(-q^2\alpha t\right)\right] \\ + B\sin\left(2\pi f t + \theta\right)\exp\left(-t/\tau\right) + C, \end{aligned} \tag{12}$$

where A, B, and C are amplitude constants, f is the frequency of the acoustic oscillation, θ is the acoustic phase, and τ is the acoustic decay constant. In this fit the free parameters are A, B, C, α, β, θ, and τ. The acoustic frequency f is not taken as a free parameter, unlike the procedure followed by Hofmann et al., as that frequency is easily identifiable by analyzing the power spectrum of the measured response (see Fig. 3). For each fit, that frequency and the grating wave vector, q, are provided as fixed parameters.

Similar to the estimation steps taken for the parameters α and β prior to complete non-linear optimization, the acoustic decay parameter τ may be estimated by one of several methods and provided as a start point for the fit to Eq. (12). First, this decay time may be estimated from the Q-factor of the power spectrum of each measurement. The Q factor is computed by fitting the peak in the power spectrum to a Lorentzian to extract the full-width at half maximum, Δf, and peak frequency f_0. As $Q = f_0/\Delta f$ the decay time is then computed as

$$\tau = \frac{Q}{\pi f_0} = \frac{1}{\pi \Delta f}. \tag{13}$$

However, for measurements made on materials with non-lossy acoustic modes, such as the pure surface acoustic wave modes measured here, the acoustic decay should be dominated by the 'walk-off' effect. Namely, as the two counter-propagating acoustic waves which comprise the standing surface acoustic wave under investigation propagate out of the excitation area, that standing wave intensity decays [28]. If the beam spot size in the wave propagation dimension is given by $2a$, then the walk-off time will be $\tau \approx a/v_g$, where v_g is the group velocity of the acoustic mode in question. For the measurements conducted here on single crystal Ge, the surface acoustic wave modes should be nearly dispersionless, meaning that we have the ability to estimate the walk-off time from the phase velocity, v_p, measured directly in experiment as

$$\tau = \frac{a}{v_p} = \frac{a}{f_0 \Lambda}. \tag{14}$$

Fits using either of these estimations as starting points for the final optimization may be used, and either may perform better depending on the conditions of the experiment and the character of the acoustic modes present. For this work, a constant fixed starting value, the walk-off estimation, and the Lorentzian fit estimation for τ were found to produce identical final results. The walk-off and Lorentzian fit estimations for tau were both found to slightly under-predict the final optimized value with the walk-off estimate on average being closer. For the data presented below, we have used the walk-off estimation method for all analysis to further remove arbitrarily-chosen fitting parameters.

IV. RESULTS AND DISCUSSION

In the analysis of phase grating thermal transport measurements, the primary challenge arises from the necessity of choosing a time at which to begin the fit of either Eq. (6) or Eq. (12) to experimental data. In previous studies using amplitude grating measurements to determine thermal diffusivity, the choice of fit start time is not complicated by the presence of an acoustic oscillation. The choice is determined, rather, by noting that the $t^{-1/2}$ dependence in Eq. (2) arises due to a contribution from cross-plane diffusivity into the bulk of the material and not from the in-plane diffusion of heat from grating peak to trough. In these cases, good fits to experimental data may be found simply by starting the fit late enough to not be influenced by the divergence in Eq. (2) at $t = 0$, and therefore a fixed starting point may be chosen which is appropriate for a wide range of measurements.

This singular choice of fitting start time it not appropriate when fitting phase grating TGS measurements. Fig. 4 shows the variation in the final best-fit value of effective thermal diffusivity found using both Eq. (6) and Eq. (12) as a function of the fit start point on the {111} Ge sample, measured at 6.4 µm. The point $t = 0$ is calibrated as the time of laser impulse, determined in this case by location of the peak intensity in amplitude grating measurements made in this geometry, as in Fig. 3. This point is determined by experiment optical geometry and electronic settings and may reasonably be characterized once for a series of measurements. For fits conducted both with and without a sinusoidal variation, the best-fit value of α is initially underestimated at very short time scales. Following the rapid increase in best-fit value, the fit values saturate and then oscillate fairly consistently. In both cases, these oscillations in diffusivity value occur at the same period as the acoustic oscillation present, in this case at 2.28 ns. For fits to Eq. (6), oscillations in α are out-of-phase with the acoustic oscillation, i.e. maxima in the fit value of the effective diffusivity do not correspond to maxima in the recorded signal. In contrast, fits to Eq. (12) show smaller amplitude oscillations which are in-phase with the acoustic oscillations in the recorded signal.

After the initial saturation period, for the example trace in Fig. 4 the deviation in the best-fit value for α over one acoustic period is $\Delta\alpha/\alpha = 9.3\%$ when fitting to Eq. (6). When fitting to Eq. (12), this deviation over one period is reduced to $\Delta\alpha/\alpha = 3.5\%$. This trend of a reduction in deviation with the inclusion of a decaying sinusoidal term is consistent across phase grating data at different grating spacings. It is also consistent with the work of Hofmann et al., who noted a reduction in this deviation from 6% to 1% when including the same oscillatory term [13]. The poorer performance in the case presented here is likely due to the added complexity of the non-negligible reflectivity component in the phase grating response. Nevertheless, the reduction in deviation using Eq. (12) strongly motivates the use of this form to

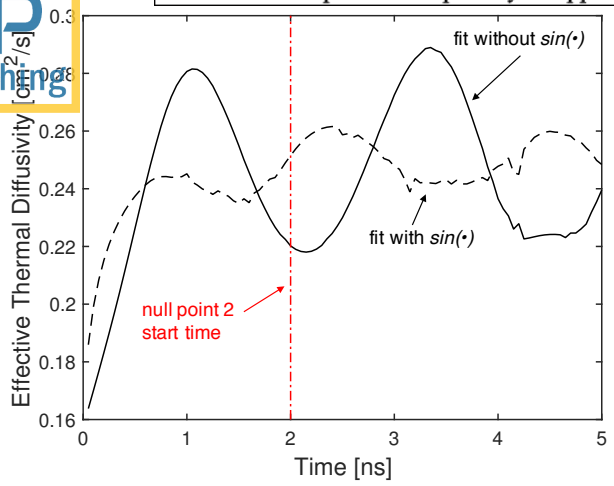

FIG. 4. Variation in best fit value of α with changing fit start time for measurement at 6.4 µm grating spacing on {111} oriented Ge. The solid line is the best-fit value using Eq. (6) and the dashed line is the best-fit value using Eq. (12). An initial saturation period followed by oscillation in α at the acoustic frequency are characteristic features observed for all measurements. The vertical line denotes the final null-point start time chosen for this measurement.

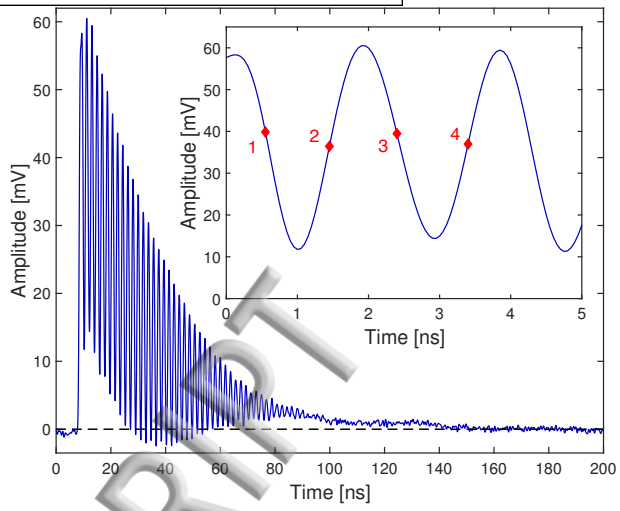

FIG. 5. 5.5 µm grating spacing measurement on {001} Ge with the inset showing the first 5 ns of the trace, rescaled in time to the laser impulse. The first four null-point points are labeled on the inset to indicate where start times for model fitting may be chosen. The scale is in millivolts as measured on a pair of Si avalanche photodiodes.

fit phase grating data of this type.

The total uncertainty on thermal diffusivity values measured using amplitude gratings is reported by Johnson et al. to be in the range of 2-3% [1], making the performance variation shown in Fig. 4 less than ideal. One method of combating this variation would be, for every measurement analyzed, to perform a series of fits to the data using sequential start times over one acoustic oscillation period following the saturation period. The average of these sequential fits could then be used as the 'best-fit' value for the measurement. This procedure is potentially quite computationally expensive, especially for measurements with low frequency acoustic oscillations.

Instead, a fixed null-point start time selection criterion may be established to provide results that are consistent with averages made over an entire acoustic period. Fig. 5 describes these null points by showing both a complete measurement made at 5.5 µm on a {001} Ge sample in addition to an insert showing the first 5 ns of the same trace after shifting $t = 0$ to the laser impulse time. The null-points in the inset are computed as mid-points of sequential maxima and minima in the recorded measurements. Since the oscillations in best-fit values of α are found to be in phase with recorded acoustic oscillations, these null-points are good indications of the mean value of the oscillation shown in Fig. 4. Therefore, by picking one of these null-points as the start position of the fits to Eq. (12) a self-consistent best choice fit start point may be selected individually for each measurement analyzed.

The performance of each null-point start may be evaluated, in this case, by direct comparison of the extracted effective thermal diffusivity to that calculated using the method of Huberman et al. This comparison indicates that the choice of null-point 2, as indicated in Fig. 5, is the most consistently appropriate choice for start times for fits to this type of phase grating data. For the example measurement analyzed in Fig. 4, this null-point start time is $t_2 = 2.00$ ns, and is indicated by the dashed vertical line on that plot. For that trace, the best-fit effective thermal diffusivity is $\alpha = 0.252 \pm 0.003$ cm^2/s, where the uncertainty is the 1σ confidence interval on the fit value. In comparison, the average value of the effective thermal diffusivity fit using Eq. (12), taken over one acoustic period using t_2 as the center point, is $\alpha = 0.248 \pm 0.009$ cm^2/s, indicating that the null-point 2 start does in fact capture the behavior of the period-averaged effective thermal diffusivity accurately.

Null-point 2, therefore, is taken as the start point of choice and each TGS measurement is analyzed using a fit to Eq. (12) following parameter pre-computation as described in Section III C. The exception to this proscription is the data collected at $\Lambda_0 = 3.6$ µm on the {111} oriented sample. That series of measurements includes an intensity spike which is large compared to the oscillation intensity at the time of the pump laser impulse. This feature interferes with optimization to Eq. (12) at short times. As a consequence, those ten measurements are fit using a null-point 3 start instead of null-point 2. The average and standard deviation in fit start times for each grating spacing are given in Table I. The deviation in start times for 4.8 and 6.4 µm measurement are relatively greater than those for the 5.5, 8.5, and 9.8 µm measurements as the location of the null-points depends on the principle acoustic frequency of each measurement, and this frequency will change as a function of crystal sur-

Grating spacing [µm]	Final fit start time [ns]
3.6	1.11 ± 0.35
4.8	1.36 ± 0.05
5.5	1.48 ± 0.03
6.4	2.01 ± 0.05
8.5	2.79 ± 0.02
9.8	3.21 ± 0.02

TABLE I. Average fit start times used for TSG measurement at each grating spacing used on pure Ge. All measurements use a null-point 2 start except for one third of the measurements made at 3.6 µm which use a null-point 3 start, leading to the relatively large variation.

face and direction. For measurements made at 3.6 µm, the large variation in start time is due to the third of the data set using null-point 3 as opposed to null-point 2. Nevertheless, this start time is extremely consistent across measurements at a given grating spacing and null-point; the deviation for each value of Λ at a fixed null-point is less than or equal to the oscilloscope time step of 0.05 ns.

Using this framework, the best-fit effective thermal diffusivity, taken as the average of 30 measurements at each grating spacing, is shown in Fig. 6 plotted versus the calculated value for 1D thermal transport at each wavelength. Here, averages which are taken over three Ge crystal orientations, $\langle 100\rangle\{001\}$, $\langle 11\bar{1}\rangle\{011\}$, and $\langle 11\bar{2}\rangle\{111\}$, are indicated by diamond symbols and averages of measurements made only on the {001} oriented sample are indicated with circles. Calculations of the 1D effective thermal conductivity from the BTE are converted to thermal diffusivity using standard values for Ge density and heat capacity at room temperature [29]. These experimentally determined values for effective thermal diffusivity agree well with those predicted by the model. Error bars are given as the standard deviation of the spatially averaged data points at each grating spacing. Calculated in this way, errors range from a maximum of $\Delta\alpha/\alpha = 7.2\%$ for measurement at 6.4 µm to a minimum of 1.7% at 8.5 µm. Averages which are taken over multiple samples consistently show larger deviations, which is to be expected.

In addition to the final best-fit values for thermal diffusivity, it is also instructive to inspect the best-fit profiles to each measurement. Example experimental traces with two forms of the best-fit profile are shown for each grating spacing in Fig. 7. These plots show both the final fit for the data using Eq. (12) as well as profiles generated using all the same best-fit parameters, except for setting the sinusoidal decay constant to $\tau = 0$. This has the effect of generating a profile that appears to trace the centroid of the acoustic oscillation. It is perhaps easier to qualitatively judge the performance of the fit profile in this manner. Fits reproduce the measured behavior quite well in general. The one parameter that visually does not fit as well is the acoustic decay parameter, τ.

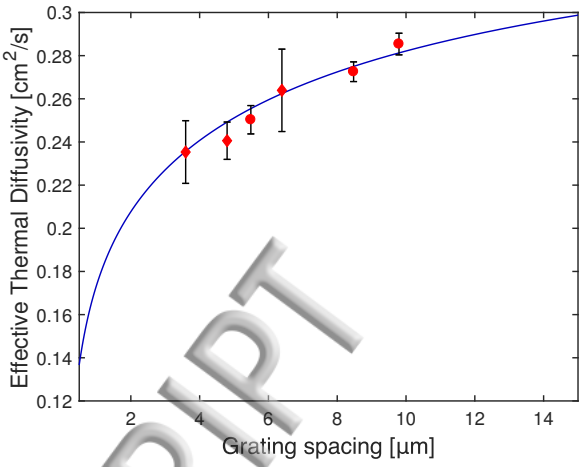

FIG. 6. Average best-fit effective thermal diffusivity versus applied grating wavelength, Λ. Diamonds symbols indicate measurements taken on three Ge crystals at different orientations and circles indicate measurements taken only on the {001} Ge crystal. The solid line indicates the expected thermal diffusivity at these wavelength calculated using a variational solution to the BTE.

The exponentially decaying term in Eq. (12) is currently a phenomenological model. Deviations from that behavior in particular are not considered physically significant in this analysis and further investigation into the governing mechanisms of that decay may yield more appropriate models.

The optimization methods developed here have only considered TGS phase grating responses containing one dominant acoustic mode. However, responses with multiple acoustic modes are often seen in practice, for example Lamb modes in thin films or pseudo-surface acoustic modes in anisotropic crystals [3,30]. For multi-mode propagation, appropriate terms would need to be added to Eq. (12) for each mode, and a systematic study conducted to determine a generalized n-mode null-point start criterion.

V. CONCLUSIONS

This work has explored the use of phase grating TGS measurements in determining thermal transport properties of opaque materials. Major takeaways from the analytical and experimental work carried out here include:

- Phase grating TGS measurements have thermal responses characteristics which are insensitive to small changes in heterodyne phase. This allows for characterization without careful control of the absolute heterodyne phase, easing previous practical experimental constraints.

- Best-fit profiles to phase grating data should use

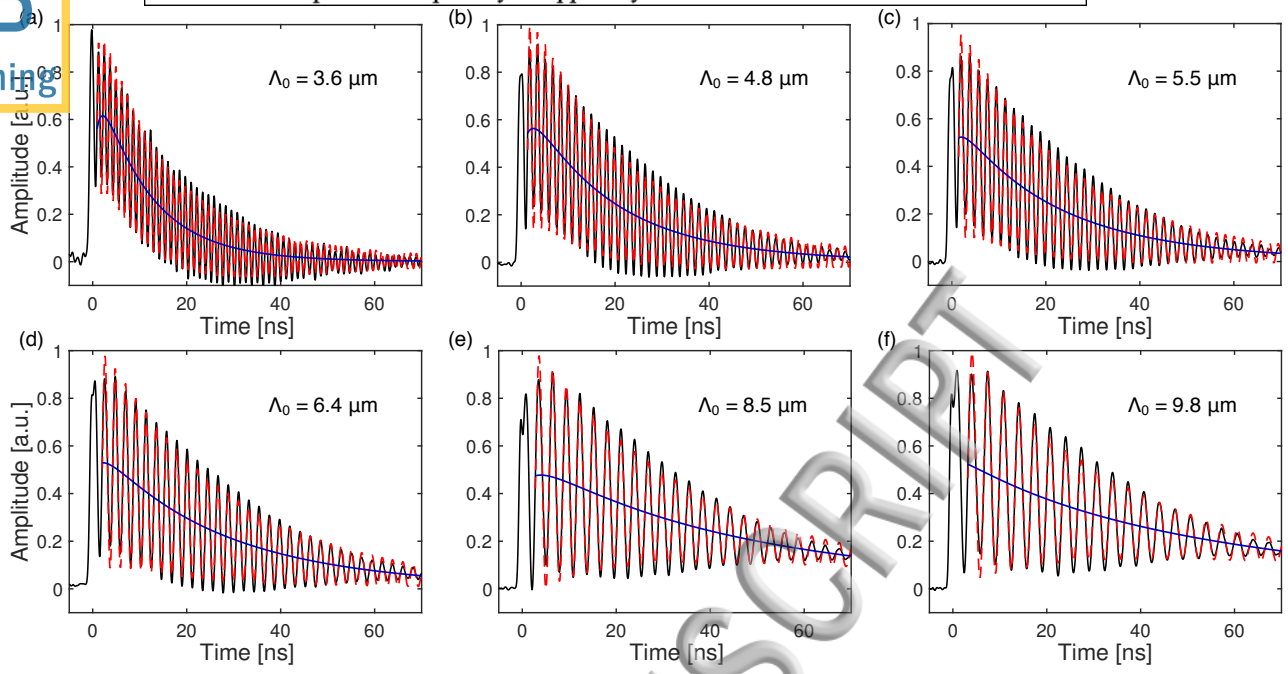

FIG. 7. Measured TGS phase grating response (solid black) and model with optimized parameters including acoustic oscillations (red dashed) and excluding oscillations (solid blue). Model fits excluding acoustic oscillations are computed using the same best-fit parameters, but setting the decay constant to $\tau = 0$. All data are recorded in a 200 ns window, which is shortened here to highlight features at short times. (For interpretation of references to color, please refer to the online version of this article).

the form of Eq. (12) to minimize the effect of acoustic oscillations on the final value of α.

- Using the characteristic maximum at t_0, model parameters may be estimated in the case that prior information regarding the thermal performance of materials under study is unavailable.
- A fixed null-point start time method allows for self-consistent fitting to measurements made with different acoustic periods without the need for performing many fits over an entire acoustic period.
- Thermal characterization carried out using these best practices can capture wavelength-dependent thermal transport in germanium with spatially averaged errors on the order of a factor of two greater than amplitude grating TGS characterization.

It is important to recall that the motivation for using the phase grating response is the presence of the acoustic component of the surface displacement which it contains. By using the best practices delineated here, both acoustic (and therefore elastic) property determination and thermal transport determination may be carried out concurrently on a wide variety of materials. This ability is a particularly powerful tool when coupled to experimental TGS implementations designed as time-resolved diagnostics for dynamically changing materials systems. Given the non-contact and non-destructive nature of TGS interrogation, the possibilities for future study using these methods are extremely broad.

ACKNOWLEDGMENTS

The authors would like to thank S. Huberman for providing the results of BTE calculations for 1D thermal transport in pure Ge and P.W. Stahle for help in the design of the vacuum experimental facility. This work is supported by the the DOE NNSA Stewardship Science Graduate Fellowship under cooperative agreement No. DE-NA0002135 and the MIT-SUTD International Design Center (IDC). M.P.S. acknowledges funding from the US Nuclear Regulatory Commission's MIT Nuclear Education Faculty Development Program under Grant No. NRC-HQ-84-15-G-0045.

[1] J. A. Johnson, A. A. Maznev, M. T. Bulsara, E. A. Fitzgerald, T. C. Harman, S. Calawa, C. J. Vineis, G. Turner, and K. A. Nelson, "Phase-controlled, heterodyne laser-induced transient grating measurements of thermal transport properties in opaque material," J. Appl. Phys **111** (2012).

[2] J. Fivez, "The determination of the elastic constants of isotropic solids by means of transient thermal surface

gratings," J. Appl. Phys. **119**, 015301 (2016).
[3] J. A. Rogers, A. A. Maznev, M. J. Banet, and K. A. Nelson, "Optical generation and characterization of acoustic waves in thin films: Fundamentals and applications," Annu. Rev. Mater. Sci. **30**, 117–157 (2000).
[4] J. A. Johnson, A. A. Maznev, J. Cuffe, J. K. Eliason, A. J. Minnich, T. Kehoe, C. M. S. Torres, G. Chen, and K. A. Nelson, "Direct measurement of room-temperature nondiffusive thermal transport over micron distances in a silicon membrane," Phys. Rev. Lett. **110**, 025901 (2013).
[5] B. Verstraeten, J. Sermeus, R. Salenbien, J. Fivez, G. Shkerdin, and C. Glorieux, "Determination of thermoelastic material properties by differential heterodyne detection of impulsive stimulated thermal scattering," Photoacoustics **3**, 64–77 (2015).
[6] A. Vega-Flick, R. A. Duncan, J. K. Eliason, J. Cuffe, J. A. Johnson, J.-P. M. Peraud, L. Zeng, Z. Lu, A. A. Maznev, E. N. Wang, J. J. Alvarado-Gil, M. Sledzinska, C. M. Sotomayor Torres, G. Chen, and K. A. Nelson, "Thermal transport in suspended silicon membranes measured by laser-induced transient gratings," AIP Advances **6**, 121903 (2016).
[7] J. Janusonis, T. Jansma, C. L. Chang, Q. Liu, A. Gatilova, A. M. Lomonosov, V. Shalagatskyi, T. Pezeril, V. V. Temnov, and R. I. Tobey, "Transient grating spectroscopy in magnetic thin films: Simultaneous detection of elastic and magnetic dynamics," Sci. Rep. **6**, 29143 (2016).
[8] N. Gedik, J. Orenstein, Ruixing Liang, D. A. Bonn, and W. N. Hardy, "Diffusion of nonequilibrium quasiparticles in a cuprate superconductor," Science **300**, 1410–1412 (2003).
[9] L. Yang, J. D. Koralek, J. Orenstein, D. R. Tibbetts, J. L. Reno, and M. P. Lilly, "Measurement of electron-hole friction in an n-doped GaAs/AlGaAs quantum well using optical transient grating spectroscopy," Phys. Rev. Lett. **106**, 247401 (2011).
[10] N. Boechler, J. K. Eliason, A. Kumar, A. A. Maznev, K. A. Nelson, and N. Fang, "Interaction of a contact resonance of microspheres with surface acoustic waves," Phys. Rev. Lett. **111**, 036103 (2013).
[11] S. Huberman, V. Chiloyan, R. A. Duncan, L. Zeng, R. Jia, A. A. Maznev, E. A. Fitzgerald, K. A. Nelson, and G. Chen, "Unifying first-principles theoretical predictions and experimental measurements of size effects in thermal transport in sige alloys," Phys. Rev. Materials **1**, 054601 (2017).
[12] F. Hofmann, D. Nguyen-Manh, M.R. Gilbert, C.E. Beck, J.K. Eliason, A.A. Maznev, W. Liu, D.E.J. Armstrong K.A. Nelsond, and S.L. Dudarev, "Lattice swelling and modulus change in a helium-implanted tungsten alloy: X-ray micro-diffraction, surface acoustic wave measurements, and multiscale modelling," Acta Mater. **89**, 352–363 (2015).
[13] F. Hofmann, D. R. Mason, J. K. Eliason, A. A. Maznev, K. A. Nelson, and S. L. Dudarev, "Non-contact measurement of thermal diffusivity in ion-implanted nuclear materials," Sci. Rep. **5**, 16042 (2015).
[14] C. A. Dennett, P. Cao, S. E. Ferry, A. Vega-Flick, A. A. Maznev, K. A. Nelson, A. G. Every, and M. P. Short, "Bridging the gap to mesoscale radiation materials science with transient grating spectroscopy," Phys. Rev. B **94**, 214106 (2016).
[15] C. A. Dennett, K. P. So, A. Kushima, D. L. Buller, K. Hattar, and M. P. Short, "Detecting self-ion irradiation-induced void swelling in pure copper using transient grating spectroscopy," Acta Mater. **145**, 496–503 (2018).
[16] R. J. Smith, W. Li, J. Coulson, M. Clark, M. G. Somekh, and S. D. Sharples, "Spatially resolved acoustic spectroscopy for rapid imaging of material microstructure and grain orientation," Meas. Sci. Technol. **25**, 055902 (2014).
[17] C. A. Dennett and M. P. Short, "Time-resolved, dual heterodyne phase collection transient grating spectroscopy," Appl. Phys. Lett. **110**, 211106 (2017).
[18] A. A. Maznev, K. A. Nelson, and J.A. Rogers, "Optical heterodyne detection of laser-induced gratings," Opt. Lett. **23**, 1319–1321 (1998).
[19] T. Grabec, P. Sedlak, P. Stoklasova, M. Thomasova, D. Shilo, M. Kabla, H. Seiner, and M. Landa, "In situ characterization of local elastic properties of thin shape memory films by surface acoustic waves," Smart Mater. Struct. **25**, 127002 (2016).
[20] X. Du and J.-C. Zhao, "Facile measurement of single-crystal elastic constants from polycrystalline samples," npj Comput. Mater. **3** (2017), http://dx.doi.org/10.1038/s41524-017-0019-x.
[21] G. Simmons and H. Wang, *Single crystal elastic constants and calculated aggregate properties: a handbook, 2nd Ed.* (MIT Press, 1971) ISBN 0262190923.
[22] J.J. More, "Levenberg–marquardt algorithm: implementation and theory," in *Conference on Numerical Analysis, University of Dundee, Scotland* (1977).
[23] C. A. Dennett and M. P. Short, http://dx.doi.org/10.5281/zenodo.1239854.
[24] O.W. Kading, H. Skurk, A.A. Maznev, and E. Matthias, "Transient thermal gratings at surfaces for thermal characterization of bulk materials and thin films," Appl. Phys. A **61**, 253–261 (1995).
[25] D. E. Aspnes and A. A. Studna, "Dielectric functions and optical parameters of Si, Ge, GaP, GaAs, GaSb, InP, InAs, and InSb from 1.5 to 6.0 eV," Phys. Rev. B **27**, 985–1009 (1983).
[26] J. A. Johnson, J. K. Eliason, A. A. Maznev, T. Luo, and K. A. Nelson, "Non-diffusive thermal transport in gaas at micron length scales," J. Appl. Phys. **118**, 155104 (2015).
[27] N. Gedik and J. Orenstein, "Absolute phase measurement in heterodyne detection of transient gratings," Opt. Lett. **29**, 2109–2111 (2004).
[28] A. A. Maznev and O. B. Wright, "Optical generation of long-lived surface vibrations in a periodic microstructure," J. Appl. Phys. **105**, 123530 (2009).
[29] L.E. Vorobyev, "Germanium (Ge)," in *Handbook Series on Semiconductor Parameters*, Vol. 1 (World Scientific, 1996) pp. 33–57.
[30] A.G. Every, A.A. Maznev, W. Grill, M. Pluta, J.D. Comins, O.B. Wright, O. Matsuda, W. Sachse, and J.P. Wolfe, "Bulk and surface acoustic wave phenomena in crystals: Observation and interpretation," Wave Motion **50**, 1197–1217 (2013).

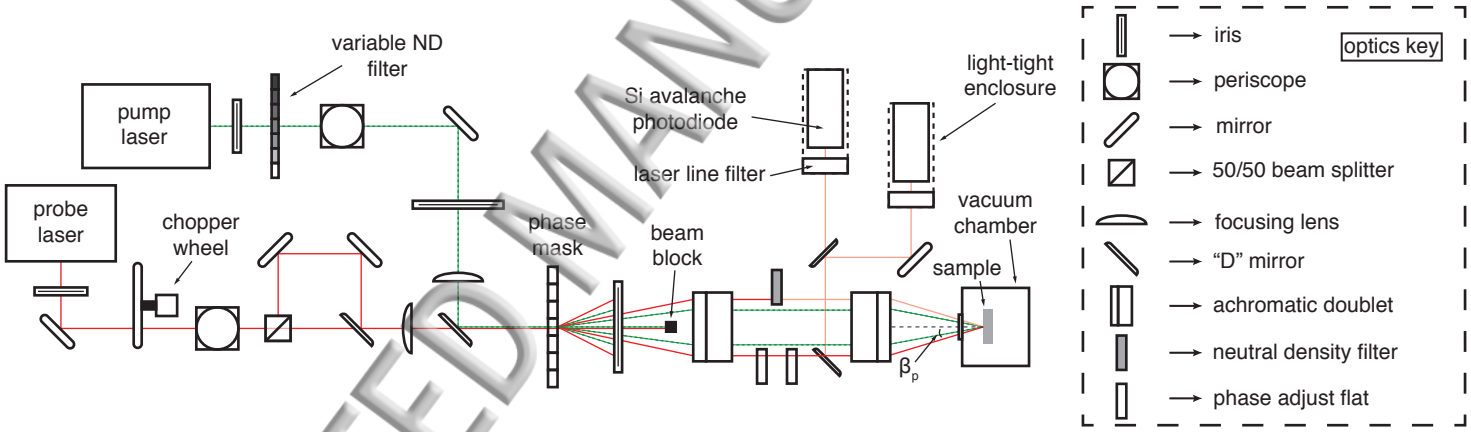
variable ND filter
pump laser
probe laser
chopper wheel
phase mask
beam block
Si avalanche photodiode
laser line filter
light-tight enclosure
vacuum chamber
sample
β_p
optics key
iris
periscope
mirror
50/50 beam splitter
focusing lens
"D" mirror
achromatic doublet
neutral density filter
phase adjust flat

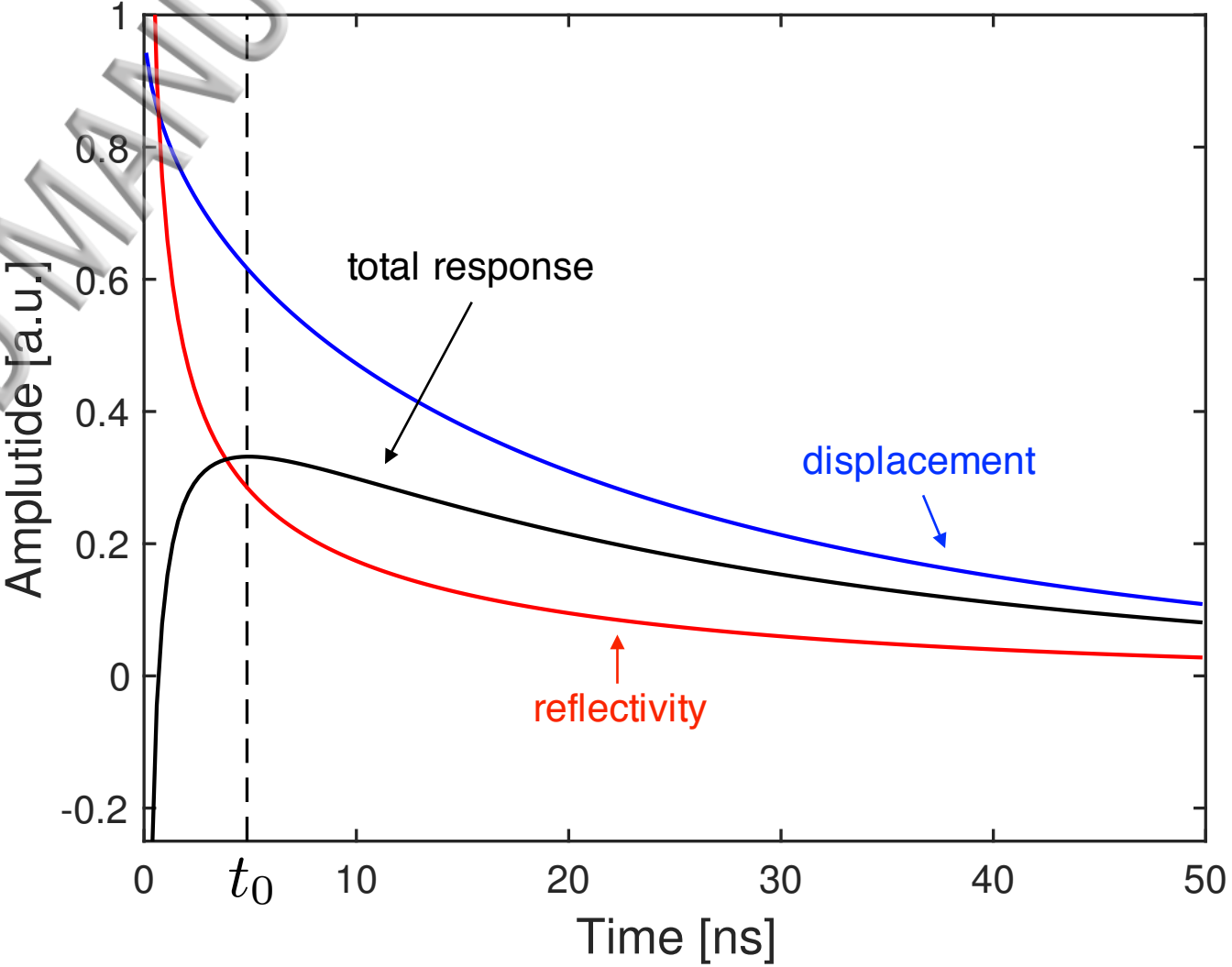
Amplutide [a.u.]
1
0.8
0.6
0.4
0.2
0
-0.2
total response
displacement
reflectivity
0
t_0
10
20
30
40
50
Time [ns]

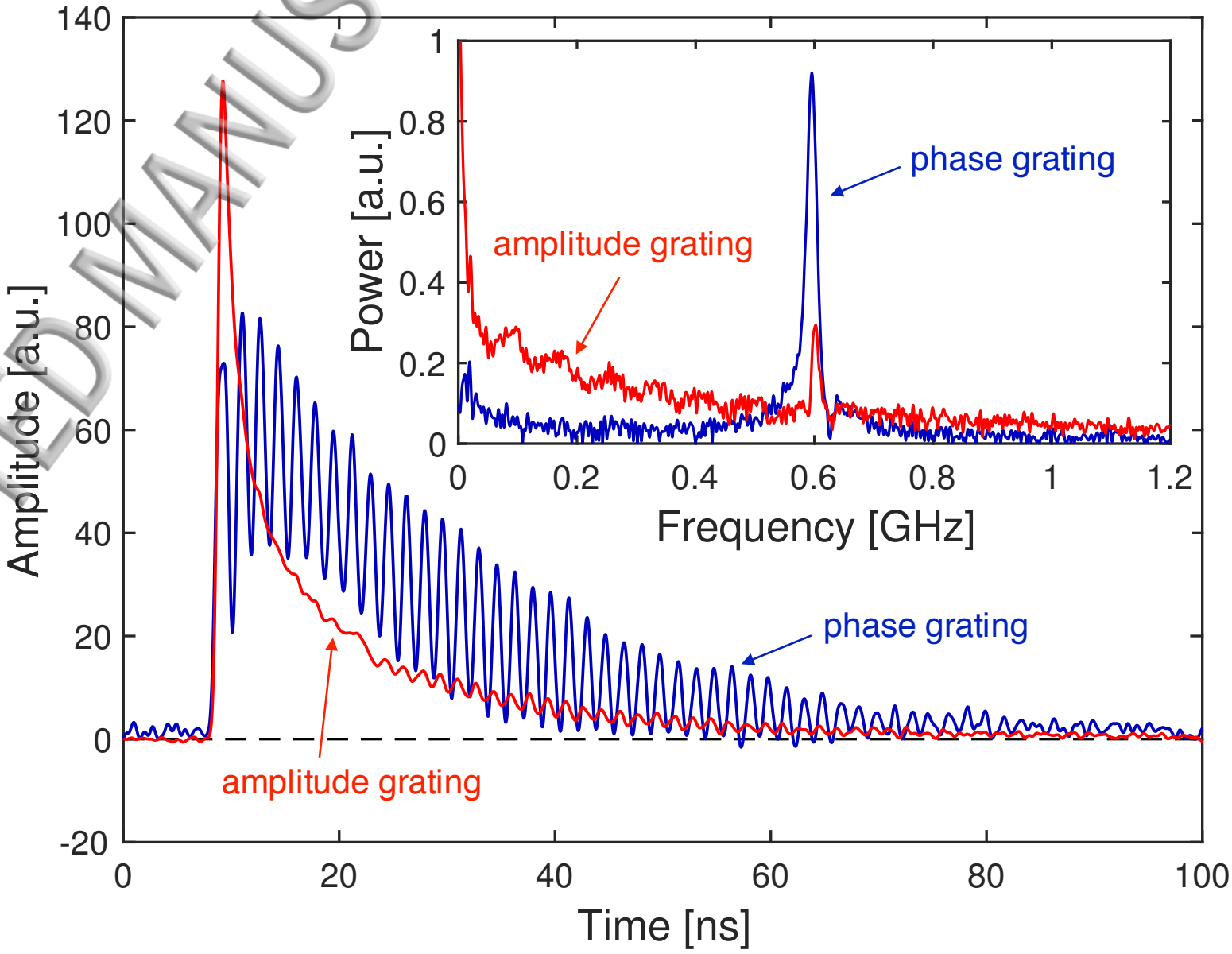
Amplitude [a.u.]
Time [ns]
phase grating
amplitude grating
Power [a.u.]
Frequency [GHz]
phase grating
amplitude grating

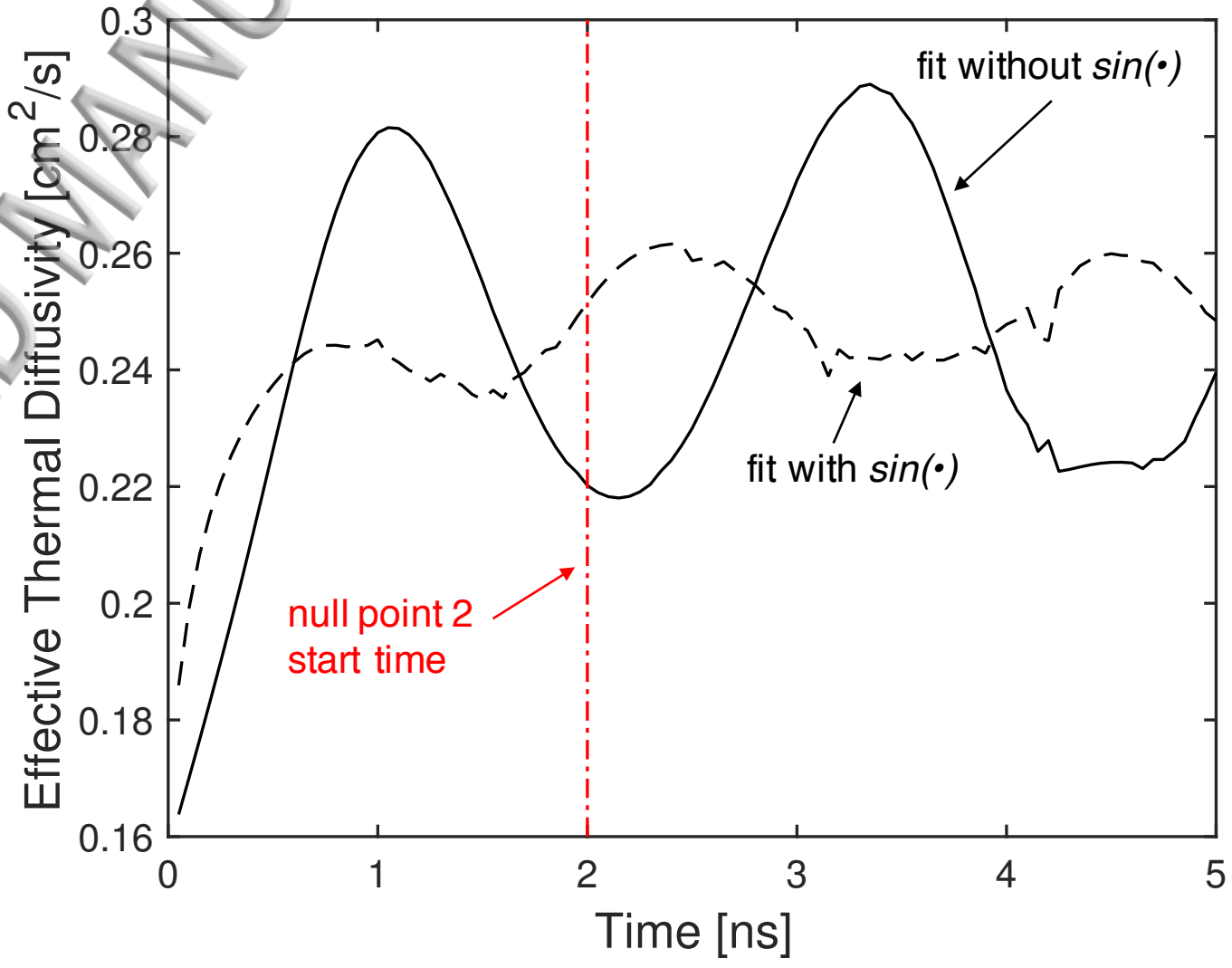
Effective Thermal Diffusivity [cm^2/s]
0.3
0.28
0.26
0.24
0.22
0.2
0.18
0.16
0
1
2
3
4
5
Time [ns]
fit without sin(•)
fit with sin(•)
null point 2
start time

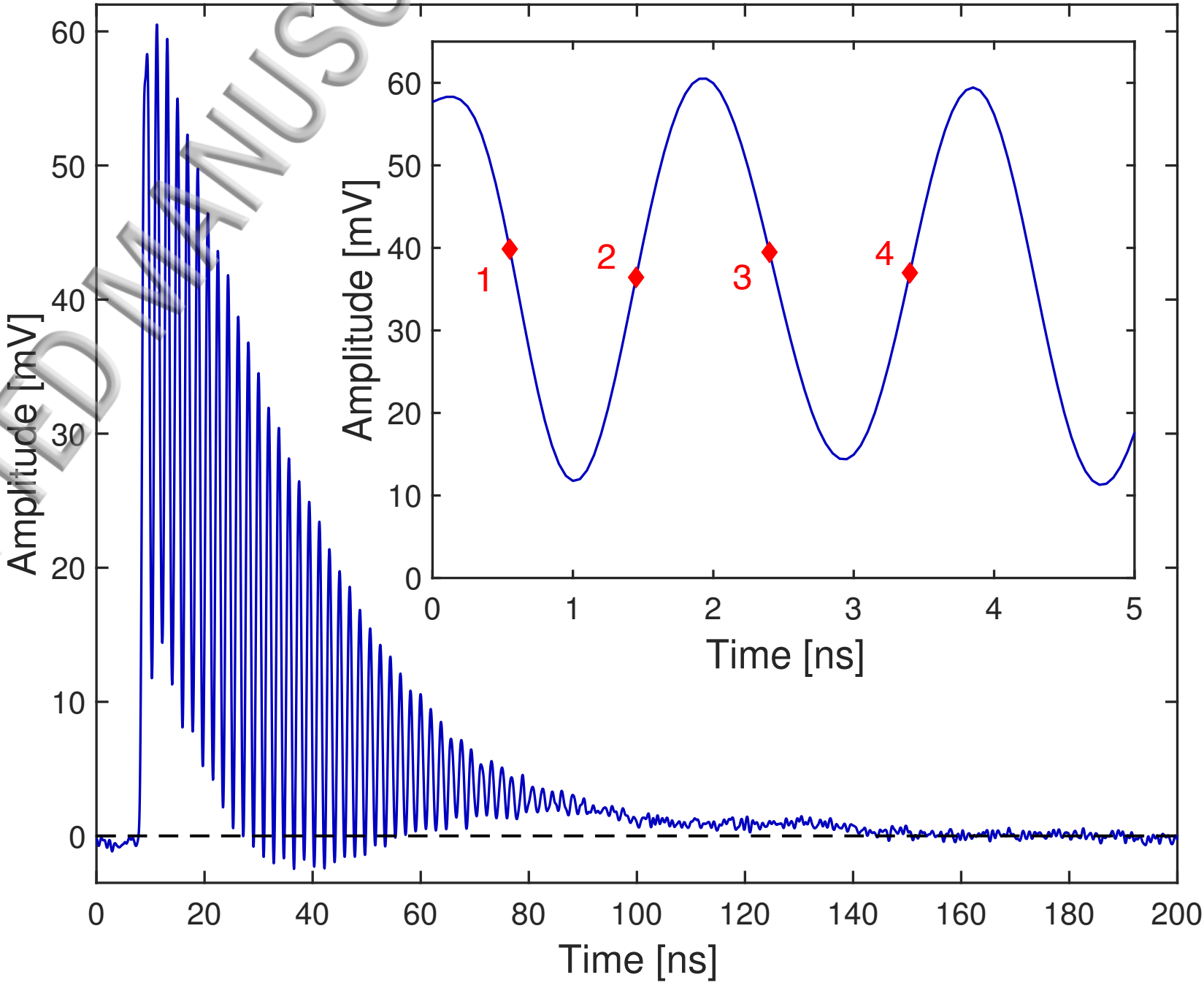
Amplitude [mV]
Time [ns]
0
10
20
30
40
50
60
0
20
40
60
80
100
120
140
160
180
200
Amplitude [mV]
Time [ns]
1
2
3
4
0
10
20
30
40
50
60
0
1
2
3
4
5

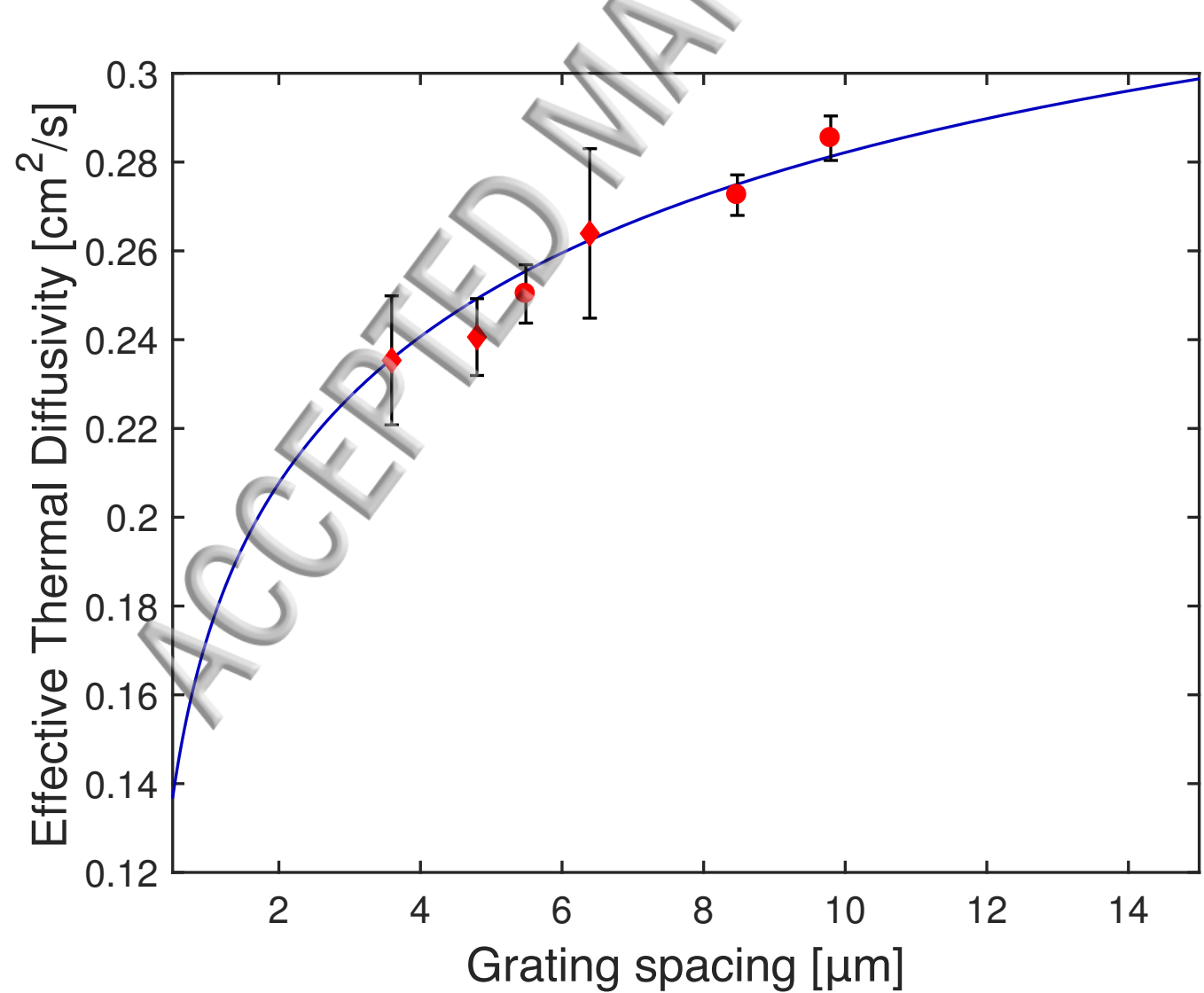
Effective Thermal Diffusivity [cm^2/s]
0.3
0.28
0.26
0.24
0.22
0.2
0.18
0.16
0.14
0.12
2
4
6
8
10
12
14
Grating spacing [μm]